

Joint Community and Anomaly Tracking in Dynamic Networks[†]

Brian Baingana, Student Member, IEEE and Georgios B. Giannakis, Fellow, IEEE*

Abstract—Most real-world networks exhibit community structure, a phenomenon characterized by existence of node clusters whose intra-edge connectivity is stronger than edge connectivities between nodes belonging to different clusters. In addition to facilitating a better understanding of network behavior, community detection finds many practical applications in diverse settings. Communities in online social networks are indicative of shared functional roles, or affiliation to a common socio-economic status, the knowledge of which is vital for targeted advertisement. In buyer-seller networks, community detection facilitates better product recommendations. Unfortunately, reliability of community assignments is hindered by anomalous user behavior often observed as unfair self-promotion, or “fake” highly-connected accounts created to promote fraud. The present paper advocates a novel approach for jointly tracking communities while detecting such anomalous nodes in time-varying networks. By postulating edge creation as the result of mutual community participation by node pairs, a dynamic factor model with anomalous memberships captured through a sparse outlier matrix is put forth. Efficient tracking algorithms suitable for both online and decentralized operation are developed. Experiments conducted on both synthetic and real network time series successfully unveil underlying communities and anomalous nodes.

Index Terms—Community detection, anomalies, non-negative matrix factorization, low rank, sparsity.

I. INTRODUCTION

Networks underlie many complex phenomena involving pairwise interactions between entities [8], [17]. Examples include online social networks such as Facebook or Twitter, e-mail and phone correspondences among individuals, the Internet, and electric power grids. Most network analyses focus on static networks, with node and link structures assumed fixed. However, real-world networks often evolve over time e.g., new links are frequently added to the web. Incorporating such temporal dynamics plays a fundamental role towards a better understanding of network behavior.

Community identification is one of the most studied tasks in modern network analysis [9], [12]. Fundamentally, communities pertain to the inherent grouping of nodes, with many edges connecting nodes belonging to the same cluster, and far fewer edges existing between clusters. Cognizant of the temporal behavior inherent to networks, several recent works have focused on the task of tracking time-varying communities [13], [18], [20], [28], [29]. Identification of dynamic communities finds

applications in many settings e.g., grouping subscribers of an online social network into functional roles for more informative advertising, or clustering blogs into content groups, facilitating improved recommendations to readers.

Classical community detection approaches predominantly resort to well-studied unsupervised machine learning algorithms e.g., hierarchical and spectral clustering [14], [16], [19]. To facilitate interpretability, several authors have postulated that a network exhibits community structure if it contains subnetworks whose expected node degree exceeds that of a random graph; see e.g., modularity [22]. Many of these methods conduct hard community assignment, whereby no node can jointly belong to more than one community. Nevertheless, communities in real networks tend to overlap with, or even completely contain others e.g., a Facebook user may jointly belong to a circle of college friends, and another comprising workplace colleagues. The quest to unveil possibly overlapping communities has been at the forefront of efforts to develop more flexible community discovery algorithms, capable of associating each node with a per-community affiliation strength a.k.a, soft clustering. Among these, factor models e.g., non-negative matrix factorization (NMF), have recently become popular for overlapping community discovery [20], [24], [30].

This paper builds upon recent advances in overlapping community identification, with focus on dynamic networks. It is assumed that temporal variations are slow across observation time intervals. In addition, special attention is paid to existence of aberrant nodes exhibiting “anomalous” behavior. Such behavior may often manifest as unusually strong, uni-directional edge connectivity across communities, leading to distortion of true communities; see Figure 1. Examples include e-mail spammers, or individuals with malicious intent, masquerading under “false” Facebook profiles to initiate to connect with as many legitimate users as possible. Anomalies identification facilitates discovery of more realistic communities. The present paper develops algorithms for jointly tracking time-varying communities, while compensating for anomalies.

Several prior works have studied the evolution of general temporal behavior in time-varying networks; see e.g., [1], [2], [7], [10], [23], [27]. Using tensor and matrix factorizations, temporal link prediction approaches are advocated for bipartite graphs in [7]. Postulating a state-space dynamic stochastic blockmodel for dynamic edge evolution, an extended Kalman filter was proposed for tracking communities in [29]. An NMF model was advocated for batch recovery of overlapping communities in time-varying networks in [20]. Generally, these contemporary approaches do not account for the occurrence of distortive anomalies, which may hurt the accuracy of community assignments.

The fresh look advocated by the present paper jointly

[†] Work in this paper was supported by NSF-EECS Grant No. 1343248 and AFOSR-MURI Grant No. FA9550-10-1-0567. Parts of the paper appeared in the *Proc. of the IEEE Global Conference on Signal and Information Processing*, Atlanta, Georgia, December 3-5, 2014.

* The authors are with the Dept. of ECE and the Digital Technology Center, University of Minnesota, 200 Union Street SE, Minneapolis, MN 55455. Tel/fax: (612)626-7781/625-4583; Emails: {baing011,georgios}@umn.edu

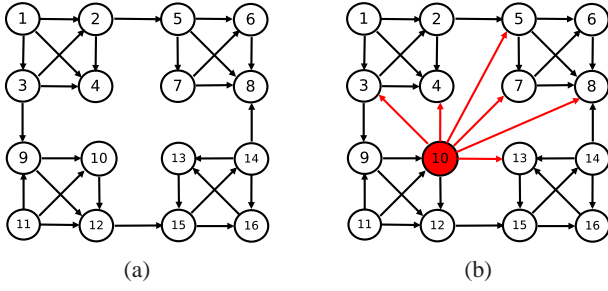


Fig. 1: An illustration of the distortive effect of anomalous nodes: a) A 16-node directed network with four easily-discernible communities; and b) The same network with node 10 exhibiting an unusually high number of outgoing edges. Identifying the underlying communities is more challenging, as a result of the distortion caused by node 10.

accounts for temporal variations and anomalous affiliations. Motivated by contemporary NMF approaches, a community affiliation model in which edge weights are generated by mutual community participation between node pairs is adopted in Section II. The proposed approach capitalizes on sparsity of anomalies, rank deficiency inherent to networks with far fewer communities than the network size, as well as slow edge variation across time intervals. Under these conditions, a sparsity-promoting, rank-regularized, exponentially-weighted least-squares estimator is put forth in Section III. Leveraging advances in proximal splitting approaches (see e.g., [4]), computationally efficient community tracking algorithms, based on alternating minimization are developed.

In order to appeal to big data contexts, within which most social networks of interest arise, a number of algorithmic modifications are considered. Towards facilitating real-time, memory-efficient operation in streaming data settings, an on-line algorithm leveraging stochastic gradient descent iterations is developed in Section IV-B. Moreover, certain practical settings entail storage of network data across many clusters of computing nodes, possibly geographically located at different sites. In such scenarios, tracking communities in a decentralized fashion is well-motivated. To this end, a tracking algorithm that leverages the alternating direction method of multipliers (ADMM) is developed in Section V. Numerical tests with synthetically generated networks demonstrate the effectiveness of the developed algorithms in tracking communities and anomalies (Section VI-A). Further experiments in Section VI-B are conducted on real data, extracted from global trade flows among nations between 1870 and 2009.

Notation. Bold uppercase (lowercase) letters will denote matrices (column vectors), while operators $(\cdot)^\top$, $\lambda_{\max}(\cdot)$, and $\text{diag}(\cdot)$ will stand for matrix transposition, maximum eigenvalue, and diagonal matrix, respectively. The identity matrix will be represented by \mathbf{I} , while $\mathbf{0}$ denotes the matrix of all zeros. The ℓ_p and Frobenius norms will be denoted by $\|\cdot\|_p$, and $\|\cdot\|_F$, respectively. The indicator function $\mathbb{1}_{\{x\}} = 1$ if x evaluates to “true”, otherwise $\mathbb{1}_{\{x\}} = 0$. Finally, $[\mathbf{X}]_+$ will denote projection of \mathbf{X} onto the non-negative orthant, with the (i, j) -th entry $[[\mathbf{X}]_+]_{ij} = \max([\mathbf{X}]_{ij}, 0)$.

II. MODEL AND PROBLEM STATEMENT

A. Community affiliation model

Consider a dynamic directed N -node network whose time-varying topology is captured by the time-series of adjacency matrices $\{\mathbf{A}^t \in \mathbb{R}^{N \times N}\}_{t=1}^T$. Entry (i, j) of \mathbf{A}^t (hereafter denoted by a_{ij}^t) is nonzero only if an edge originating from node i is connected to node j during interval t . It is assumed that edge weights are nonnegative, namely $a_{ij}^t \geq 0$. Suppose that the network consists of C unknown communities which are allowed to overlap, that is a node can belong to one or more communities simultaneously. This is motivated by practical settings where e.g., a Facebook user may be associated with multiple communities consisting of her work colleagues, former schoolmates, or friends from the local sports club. It can be reasoned that the likelihood of two people becoming friends is directly related to the number of communities to which they mutually belong. For example, if two work colleagues happen to have attended the same high school, then chances are high that they will become friends. This a fortiori argument based upon a reasonably natural observation in social settings lies at the foundation for several recent community affiliation models for edge generation [20], [30].

Suppose $\mathbf{V}^t := [\mathbf{v}_1^t \dots \mathbf{v}_C^t] \in \mathbb{R}^{N \times C}$ denotes a temporal basis matrix whose columns span a linear subspace of dimension C during observation interval t . Associating each basis vector with one of C communities, the edge vector associated with each node i can be expressed as a linear combination of $\{\mathbf{v}_c^t\}_{c=1}^C$, i.e.,

$$\mathbf{a}_i^t = \mathbf{V}^t \mathbf{u}_i^t + \mathbf{e}_i^t, \quad i = 1, \dots, N \quad (1)$$

where $(\mathbf{a}_i^t)^\top$ denotes row i of \mathbf{A}^t , and \mathbf{e}_i^t captures unmodeled dynamics. Entries of $\mathbf{u}_i^t := [u_{i1}^t \dots u_{iC}^t]^\top \in \mathbb{R}^C$ in (1) assign community affiliation strengths, with $u_{ic}^t = 0$ only if node i does not belong to community c during interval t . Since $a_{ij}^t \geq 0$, entries of both \mathbf{V}^t and \mathbf{u}_i^t will be constrained to nonnegative values. Collecting edge vectors for all nodes, (1) can be expressed equivalently as the following canonical NMF model

$$\mathbf{A}^t = \mathbf{U}^t (\mathbf{V}^t)^\top + \mathbf{E}^t \quad (2)$$

where $(\mathbf{U}^t)^\top := [\mathbf{u}_1^t \dots \mathbf{u}_N^t]$, and $(\mathbf{E}^t)^\top := [\mathbf{e}_1^t \dots \mathbf{e}_N^t]$. The asymmetry inherent to (2) generalizes traditional approaches (e.g., spectral clustering), rendering them capable of capturing communities in weighted, directed, and even bipartite graphs. The special case in which edges are undirected (i.e., $a_{ij}^t = a_{ji}^t$) can be readily realized $\mathbf{U}^t \equiv \mathbf{V}^t$.

Contemporary community detection approaches overwhelmingly focus on unipartite networks, whereby edges are allowed to exist between any pair of nodes. On the other hand, directional edges in bipartite networks only connect nodes belonging to two distinct classes. Examples include buyer-seller networks existing in online applications like E-bay, or recommender networks with edges capturing ratings of products by customers. With matrices $\mathbf{U}^t \in \mathbb{R}^{N \times C}$, and $\mathbf{V}^t \in \mathbb{R}^{M \times C}$, communities in an NM -node bipartite network (N nodes belonging to one class, and M to the other) can be readily captured through the affiliation model (2).

Unfortunately, (1) does not effectively capture anomalous nodes that exhibit unusually strong affiliation to one or more communities. This aberrant behavior has been observed in several real-world networks, and it often arises due to any of several reasons. For example, the presence of “fake” user accounts in online social networks created for phishing purposes from unsuspecting peers may lead to abnormally high numbers of outgoing links. In addition, fraudulent reviewers in web-based rating applications may exhibit abnormal affiliation while unfairly promoting their services to specific communities. Regardless of the underlying reason, detection of such nodes is envisioned as a source of strategic information for network operators. Moreover, identification of anomalies is critical for improved community detection accuracy; see Figure 1 for an example where an anomalous node distorts the underlying community structure.

B. Outlier-aware community affiliation model

Suppose node i is considered anomalous, exhibiting an abnormally strong level of affiliation in one or more of the C communities. In order to preserve the estimation accuracy of community discovery algorithms, one is motivated to modify (1) so that such outliers are accounted for. The present paper postulates the following robust edge generation model

$$\mathbf{a}_i^t = \mathbf{V}^t(\mathbf{u}_i^t + \mathbf{o}_i^t) + \mathbf{e}_i^t, \quad i = 1, \dots, N \quad (3)$$

where $\mathbf{o}_i^t := [o_{i1}^t \dots o_{iC}^t]^\top$, and $o_{ic}^t \neq 0$ only if node i exhibits anomalous affiliation in community c . Intuitively, (3) reasonably suggests that one can investigate whether any node is an anomaly or not by introducing more variables that compensate for the effect of outliers on the edge generation model. Since outliers are rare by definition, vectors $\{\mathbf{o}_i^t\}_{i=1}^N$ are generally sparse, and this prior knowledge can be exploited to recover the unknowns.

Letting $(\mathbf{O}^t)^\top := [\mathbf{o}_1^t \dots \mathbf{o}_N^t]$, the outlier-aware community affiliation model in (2) can be written as

$$\mathbf{A}^t = (\mathbf{U}^t + \mathbf{O}^t)(\mathbf{V}^t)^\top + \mathbf{E}^t, \quad t = 1, 2, \dots \quad (4)$$

where \mathbf{O}^t is sparse. In static scenarios with $\mathbf{A} = (\mathbf{U} + \mathbf{O})\mathbf{V}^\top$, setting $\mathbf{O} = \mathbf{0}$ yields the canonical NMF model for community discovery. Given $\{\mathbf{A}^t\}_{t=1}^T$, the goal of this paper is to track the community affiliation matrices $\{\mathbf{U}^t, \mathbf{V}^t\}_{t=1}^T$, as well as outliers captured through matrices $\{\mathbf{O}^t\}_{t=1}^T$.

It is worth reiterating that (4) is a heavily under-determined model, and the only hope to recover $\{\mathbf{U}^t, \mathbf{O}^t, \mathbf{V}^t\}_{t=1}^T$ lies in exploiting prior information about the structure of the unknowns. Indeed, the estimator advocated in the sequel will capitalize on sparsity, low rank, and the slow evolution of networks. Introducing extra variables to capture outliers has been used in different contexts; see e.g., [11] and references therein.

Remark 1 (Measurement outliers): Model 4 is motivated by anomalous nodes, whose presence leads to distorted community structures in e.g., social networks. A slight variation of this problem arises in cases where one is interested in identifying which edges are anomalous. This is well-motivated in settings where edge weights are directly measured, and encode valuable information e.g., star ratings in online review systems. The

outliers in such cases are the result of faulty measurements, bad data (e.g., skewed user ratings), or data corruption. To detect anomalous edge weights, one can postulate that [cf. (4)]

$$\mathbf{A}^t = \mathbf{U}^t(\mathbf{V}^t)^\top + \mathbf{O}^t + \mathbf{E}^t, \quad t = 1, 2, \dots \quad (5)$$

where \mathbf{O}^t is sparse, and can be effectively recovered by leveraging sparsity-promoting estimation approaches; see e.g., [11] and references therein.

III. COMMUNITY TRACKING ALGORITHM

This section assumes that the following hold: a1) \mathbf{O}^t is sparse; a2) $\mathbf{U}^t(\mathbf{V}^t)^\top$ is low rank; and a3) $\{\mathbf{A}^t\}_{t=1}^T$ evolve slowly over time, that is, the sequence of matrices $\{\mathbf{A}^t - \mathbf{A}^{t-1}\}_{t=1}^T$ are sparse. In order to justify a1, note that the set of anomalous nodes is much smaller than that of “ordinary” nodes. On the other hand, a2 results from requiring that $\text{rank}(\mathbf{U}^t(\mathbf{V}^t)^\top) \leq C \ll N$, while a3 is motivated by observations of the evolution of most real-world networks. In the sequel, a sequential estimator that exploits a1-a3 is put forth.

A. Exponentially-weighted least-squares estimator

Suppose data are acquired sequentially over time, and storage memory is limited; thus, it is impractical to aim for batch estimation. Under the aforementioned assumptions, the following sparsity-promoting, rank-regularized, and exponentially-weighted least-squares (EWLS) estimator can track the unknown matrices

$$\begin{aligned} & \{\hat{\mathbf{U}}^t, \hat{\mathbf{V}}^t, \hat{\mathbf{O}}^t\} \\ &= \arg \min_{\{\mathbf{U}, \mathbf{V}, \mathbf{O}\} \in \mathbb{R}_+^{N \times C}} \sum_{\tau=1}^t \beta^{t-\tau} \|\mathbf{A}^\tau - (\mathbf{U} + \mathbf{O})\mathbf{V}^\top\|_F^2 \\ & \quad + \lambda_t \|\mathbf{U}\mathbf{V}^\top\|_* + \mu_t \|\mathbf{O}\|_0 \end{aligned} \quad (6)$$

where the nuclear norm $\|\mathbf{U}\mathbf{V}^\top\|_* := \sum_n \sigma_n(\mathbf{U}\mathbf{V}^\top)$ sums the singular values of $\mathbf{U}\mathbf{V}^\top$, while $\|\mathbf{O}\|_0 := \sum_{ik} \mathbb{1}_{\{o_{ik} \neq 0\}}$ counts the non-zero entries in \mathbf{O} . Regularization parameters $\lambda_t \geq 0$ and $\mu_t \geq 0$ control the low rank of $\mathbf{U}\mathbf{V}^\top$ and sparsity in \mathbf{O} , respectively. Finally, $\beta^{t-\tau}$ is a “forgetting” factor with $\beta \in (0, 1]$, which facilitates tracking slow variations by down-weighting past data when $\beta < 1$.

Problem (6) is non-convex and NP-hard to solve. Nevertheless, this can be circumvented by resorting to tight convex relaxation. Specifically, $\|\mathbf{O}\|_0$ can be surrogated with $\|\mathbf{O}\|_1 := \sum_{ic} |o_{ic}|$, and one can leverage the following characterization of the nuclear norm; see e.g., [21]

$$\|\mathbf{Z}\|_* := \min_{\mathbf{U}, \mathbf{V} \in \mathbb{R}^{N \times C}} \frac{1}{2} \left\{ \|\mathbf{U}\|_F^2 + \|\mathbf{V}\|_F^2 \right\} \quad \text{s.t. } \mathbf{Z} = \mathbf{U}\mathbf{V}^\top \quad (7)$$

which leads to the following optimization problem

$$\begin{aligned} & \{\hat{\mathbf{U}}^t, \hat{\mathbf{V}}^t, \hat{\mathbf{O}}^t\} \\ &= \arg \min_{\{\mathbf{U}, \mathbf{V}, \mathbf{O}\} \in \mathbb{R}_+^{N \times C}} \sum_{\tau=1}^t \beta^{t-\tau} \|\mathbf{A}^\tau - (\mathbf{U} + \mathbf{O})\mathbf{V}^\top\|_F^2 \\ & \quad + \frac{\lambda_t}{2} \left\{ \|\mathbf{U}\|_F^2 + \|\mathbf{V}\|_F^2 \right\} + \mu_t \|\mathbf{O}\|_1 \end{aligned} \quad (8)$$

whose separability renders it amenable to alternating minimization (AM) strategies, as discussed next.

B. Alternating minimization

Focusing on the first term of the cost in (8), note that

$$\begin{aligned} & \sum_{\tau=1}^t \beta^{t-\tau} \|\mathbf{A}^\tau - (\mathbf{U} + \mathbf{O})\mathbf{V}^\top\|_F^2 \\ &= s^t \text{Tr} \left\{ \mathbf{V}(\mathbf{U}^\top \mathbf{U} + \mathbf{O}^\top \mathbf{O})\mathbf{V}^\top + 2\mathbf{V}\mathbf{U}^\top \mathbf{O}\mathbf{V}^\top \right\} \\ & \quad - 2\text{Tr} \left\{ (\mathbf{S}^t)^\top (\mathbf{U} + \mathbf{O})\mathbf{V}^\top \right\} \end{aligned} \quad (9)$$

where $s^t := (1 - \beta^t)/(1 - \beta)$ and $\mathbf{S}^t := \mathbf{A}^t + \beta\mathbf{S}^{t-1}$ recursively accumulate past data with minimal storage requirements. Since (8) is separable across the optimization variables, one can resort to iterative AM, by alternately solving for each variable while holding the others fixed. With

$$\Phi(\mathbf{U}, \mathbf{V}, \mathbf{O}, \mathbf{S}^t, s^t) := \sum_{\tau=1}^t \beta^{t-\tau} \|\mathbf{A}^\tau - (\mathbf{U} + \mathbf{O})\mathbf{V}^\top\|_F^2 \quad (10)$$

AM iterations amount to the following per-interval updates

$$\begin{aligned} \mathbf{U}[k] &= \arg \min_{\mathbf{U} \in \mathbb{R}_+^{N \times C}} \Phi(\mathbf{U}, \mathbf{V}[k-1], \mathbf{O}[k-1], \mathbf{S}^t, s^t) \\ & \quad + (\lambda_t/2) \|\mathbf{U}\|_F^2 \end{aligned} \quad (11a)$$

$$\begin{aligned} \mathbf{V}[k] &= \arg \min_{\mathbf{V} \in \mathbb{R}_+^{N \times C}} \Phi(\mathbf{U}[k], \mathbf{V}, \mathbf{O}[k-1], \mathbf{S}^t, s^t) \\ & \quad + (\lambda_t/2) \|\mathbf{V}\|_F^2 \end{aligned} \quad (11b)$$

$$\begin{aligned} \mathbf{O}[k] &= \arg \min_{\mathbf{O} \in \mathbb{R}_+^{N \times C}} \Phi(\mathbf{U}[k], \mathbf{V}[k], \mathbf{O}, \mathbf{S}^t, s^t) \\ & \quad + \mu_t \|\mathbf{O}\|_1 \end{aligned} \quad (11c)$$

over iterations indexed by k , until convergence is achieved.

The constrained subproblems in (11a) and (11b) are convex, and can be readily solved via projected gradient (PG) iterations. Since the gradients of their cost functions are available, and the projection operator onto the nonnegative orthant is well defined, PG iterations are guaranteed to eventually converge to the optimal solution [5, p. 223]. Per iteration k , PG updates amount to setting

$$\begin{aligned} \mathbf{U}[k] &= [\mathbf{U}[k-1] - \alpha_{u,k} \nabla_{\mathbf{U}} \Phi(\mathbf{U}[k-1], \\ & \quad \mathbf{V}[k-1], \mathbf{O}[k-1], \mathbf{S}^t, s^t)]_+ \end{aligned} \quad (12)$$

$$\begin{aligned} \mathbf{V}[k] &= [\mathbf{V}[k-1] - \alpha_{v,k} \nabla_{\mathbf{V}} \Phi(\mathbf{U}[k], \\ & \quad \mathbf{V}[k-1], \mathbf{O}[k-1], \mathbf{S}^t, s^t)]_+ \end{aligned} \quad (13)$$

where $\alpha_{u,k}$ and $\alpha_{v,k}$ denote (possibly) iteration-dependent step sizes. In addition, $\nabla_{\mathbf{U}} \Phi(\cdot)$ ($\nabla_{\mathbf{V}} \Phi(\cdot)$) denotes the gradient of $\Phi(\cdot)$ with respect to \mathbf{U} (\mathbf{V}). Expressions for the gradients can be readily obtained, but are omitted here due to space constraints.

The cost function in (11c) is convex with both smooth and non-smooth terms. Recent advances in proximal algorithms have led to efficient, provably-convergent iterative schemes

Algorithm 1 Alternating minimization

```

1: Input:  $\{\mathbf{A}^t\}_{t=1}^T, \beta, C$ 
2: Initialize  $\mathbf{U}[0], \mathbf{V}[0], \mathbf{O}[0]$ 
3: Set  $\mathbf{S}^0 = \mathbf{0}$ 
4: for  $t = 1 \dots$  do
5:   Set  $s^t = (1 - \beta^t)/(1 - \beta)$ 
6:   Update  $\mathbf{S}^t = \mathbf{A}^t + \beta\mathbf{S}^{t-1}$ 
7:   Initialize  $k = 0$ 
8:   repeat
9:      $k = k + 1$ 
10:    Set  $\{\alpha_{u,k}, \alpha_{v,k}\}$ 
11:    Compute  $\mathbf{U}[k]$  via (12)
12:    Compute  $\mathbf{V}[k]$  via (13)
13:     $r = 0, \mathbf{W}_r[k] = \mathbf{O}_r[k] = \mathbf{O}[k-1], \theta_r[k] = 1$ 
14:    repeat
15:      Update  $\mathbf{X}_r[k]$  via (15)
16:       $\mathbf{O}_r[k] = [\mathcal{S}_{\mu_t/L_\Psi}(\mathbf{X}_r[k])]_+$ 
17:       $\theta_{r+1}[k] = (1 + \sqrt{1 + 4\theta_r^2[k]})/2$ 
18:      Update  $\mathbf{W}_{r+1}[k]$  via (16)
19:       $r = r + 1$ 
20:    until  $\mathbf{O}_r[k]$  converges
21:     $\mathbf{O}[k] = \mathbf{O}_r[k]$ 
22:    until  $\{\mathbf{U}[k], \mathbf{V}[k], \mathbf{O}[k]\}$  converge
23:     $\hat{\mathbf{U}}^t = \mathbf{U}[k], \hat{\mathbf{V}}^t = \mathbf{V}[k], \hat{\mathbf{O}}^t = \mathbf{O}[k]$ 
24:  end for

```

for solving such optimization problems. We will resort to the *fast iterative shrinkage thresholding algorithm (FISTA)* whose accelerated convergence rate renders it attractive for sequential learning [4].

C. FISTA for outlier updates

Note that (11c) does not admit a closed-form solution, and the proposed strategy will entail a number of inner iterations (indexed by r), per AM iteration k . FISTA solves for \mathbf{O} in (11c) through a two-step update involving gradient descent on $\Phi(\cdot)$, evaluated at a linear combination of the two most recent iterates, followed by a closed-form soft-thresholding step per iteration r . Setting $\theta_0[k] = 1$ and $\mathbf{W}_1[k] = \mathbf{O}_{k-1}$, it turns out that the updates can be written as [4]

$$\mathbf{O}_r[k] = \arg \min_{\mathbf{O} \in \mathbb{R}_+^{N \times C}} (L_\Phi/2) \|\mathbf{O} - \mathbf{X}_r[k]\|_F^2 + \mu_t \|\mathbf{O}\|_1 \quad (14)$$

where

$$\begin{aligned} \mathbf{X}_r[k] &= (\mathbf{W}_r[k] \\ & \quad - (1/L_\Phi) \nabla_{\mathbf{O}} \Phi(\mathbf{W}_r[k], \mathbf{U}[k], \mathbf{V}[k], \mathbf{S}^t, s^t)) \end{aligned} \quad (15)$$

with

$$\theta_{r+1}[k] = (1 + \sqrt{1 + 4\theta_r^2[k]})/2.$$

Furthermore,

$$\mathbf{W}_{r+1}[k] = \mathbf{O}_r[k] + \left(\frac{\theta_r[k] - 1}{\theta_{r+1}[k]} \right) (\mathbf{O}_r[k] - \mathbf{O}_{r-1}[k]) \quad (16)$$

where L_Φ denotes a *Lipschitz* constant of $\nabla_{\mathbf{O}} \Phi(\cdot)$. Note that (14) is similar to the so-termed *least-absolute shrinkage*

and selection operator (Lasso) with a closed-form solution, namely $[\mathbf{O}_r[k]]_{ij} = [\mathcal{S}_{\mu_t/L_\Phi}([\mathbf{X}_r[k]]_{ij})]_+$, where the thresholding operator is defined entry-wise as $\mathcal{S}_\mu(x) := (|x| - \mu)_+ \text{sign}(x)$ [14, Ch. 3]. Computation of $\mathbf{O}[k]$ entails solving (14) over several iterations indexed by r until convergence. Algorithm 1 summarizes the details of the developed community tracking scheme, with β and C assumed to be given as algorithm inputs.

IV. DELAY-SENSITIVE OPERATION

Algorithm 1 relies upon convergence of the unknown variables per time interval. Unfortunately, this mode of operation is not suitable for delay-sensitive applications, where decisions must be made “on the fly.” In fact, one may be willing to trade off solution accuracy for real-time operation in certain application domains. This section puts forth a couple of algorithmic enhancements that will facilitate real-time tracking, namely by premature termination of PG iterations, and leveraging the stochastic gradient descent framework.

A. Premature termination

For networks that generally evolve slowly over time, it is not necessary to run the tracking algorithm until convergence per time interval. Since a compromise can be struck between an accurate solution computed slowly and a less accurate solution computed very fast, one can judiciously truncate the number of inner iterations to k_{\max} . This premature termination is well motivated when the network topology is piecewise stationary with sufficiently long coherence time, with respect to the number of time intervals. It is then unnecessary to seek convergence per time interval since it can be argued that a “good” solution will be attained across time intervals before the topology changes. If the network topology varies in accordance with a stationary distribution, it can be demonstrated that convergence will eventually be attained, even when $k_{\max} = 1$ i.e., running a single iteration per time interval. Algorithm 2 summarizes the steps involved in this inexact tracking scheme under the special case with $k_{\max} = 1$.

Algorithm 2 Inexact alternating minimization

- 1: **Input:** $\{\mathbf{A}^t\}_{t=1}^T, \beta, C$
 - 2: Initialize $\mathbf{U}^0, \mathbf{V}^0, \mathbf{O}^0$
 - 3: Set $\mathbf{S}^0 = \mathbf{0}, \mathbf{W}^0 = \mathbf{O}^0, \theta_0 = 1$
 - 4: **for** $t = 1 \dots T$ **do**
 - 5: Set $s^t = (1 - \beta^t)/(1 - \beta)$
 - 6: Update $\mathbf{S}^t = \mathbf{A}^t + \beta \mathbf{S}^{t-1}$
 - 7: Set $\{\alpha_{u,t}, \alpha_{v,t}\}$
 - 8: $\mathbf{U}^t = [\mathbf{U}^{t-1} - \alpha_{u,t} \nabla_{\mathbf{U}} \Phi(\mathbf{U}^{t-1}, \mathbf{V}^{t-1}, \mathbf{O}^{t-1}, \mathbf{S}^t, s^t)]_+$
 - 9: $\mathbf{V}^t = [\mathbf{V}^{t-1} - \alpha_{v,t} \nabla_{\mathbf{V}} \Phi(\mathbf{V}^{t-1}, \mathbf{U}^t, \mathbf{O}^{t-1}, \mathbf{S}^t, s^t)]_+$
 - 10: $\mathbf{X}^t = (\mathbf{W}^t - \frac{1}{L_\Phi} \nabla_{\mathbf{O}} \Phi(\mathbf{W}^t, \mathbf{U}^t, \mathbf{V}^t, \mathbf{S}^t, s^t))$
 - 11: $\mathbf{O}^t = [\mathcal{S}_{\mu_t/L_\Phi}(\mathbf{X}^t)]_+$
 - 12: $\theta_t = (1 + \sqrt{1 + 4\theta_{t-1}^2})/2$
 - 13: $\mathbf{W}^t = \mathbf{O}^t + ((\theta_{t-1} - 1)/\theta_t)(\mathbf{O}^t - \mathbf{O}^{t-1})$
 - 14: **end for**
-

B. Stochastic gradient descent

Instead of premature termination, real-time operation can be facilitated by resorting to stochastic gradient descent (SGD) iterations. Let

$$\zeta_\tau(\mathbf{U}, \mathbf{V}, \mathbf{O}, \mathbf{A}^\tau) := \|\mathbf{A}^\tau - (\mathbf{U} + \mathbf{O})\mathbf{V}^\top\|_F^2 \quad (17)$$

and

$$\zeta_{\lambda_\tau, \mu_\tau}(\mathbf{U}, \mathbf{V}, \mathbf{O}) := \frac{\lambda_\tau}{2} \left\{ \|\mathbf{U}\|_F^2 + \|\mathbf{V}\|_F^2 \right\} + \mu_\tau \|\mathbf{O}\|_1 \quad (18)$$

and consider the online learning setup, where the goal is to minimize the expected cost $E\{\zeta_\tau(\mathbf{U}, \mathbf{V}, \mathbf{O}, \mathbf{A}^\tau) + \zeta_{\lambda_\tau, \mu_\tau}(\mathbf{U}, \mathbf{V}, \mathbf{O})\}$ (with respect to the unknown probability distribution of the data). The present paper pursues an online learning strategy, in which the expected cost is replaced with the empirical cost function $(1/t) \sum_{\tau=1}^t [\zeta_\tau(\mathbf{U}, \mathbf{V}, \mathbf{O}, \mathbf{A}^\tau) + \zeta_{\lambda_\tau, \mu_\tau}(\mathbf{U}, \mathbf{V}, \mathbf{O})]$ as a surrogate. Generally, SGD is applicable to separable sum-minimization settings, in which the τ -th summand is a function of the τ -th datum. To incur the least computational and memory storage costs, the SGD approach advocated here discards all past data, and solves

$$\arg \min_{\mathbf{U}, \mathbf{V}, \mathbf{O} \in \mathbb{R}_+^{N \times C}} \zeta_t(\mathbf{U}, \mathbf{V}, \mathbf{O}, \mathbf{A}^t) + \zeta_{\lambda_t, \mu_t}(\mathbf{U}, \mathbf{V}, \mathbf{O}) \quad (19)$$

per interval t , which is tantamount to solving the EWLSE upon setting $\beta = 0$. This tracking scheme is reminiscent of the popular *least mean-squares (LMS)* algorithm, that has been well-studied within the context of adaptive estimation; see e.g., [26]. With $\mathbf{Y} := [\mathbf{U} \ \mathbf{V} \ \mathbf{O}]$, a common approach to solving (19) involves the projected iteration (see e.g., [6])

$$\mathbf{Y}^t = [\mathbf{Y}^{t-1} - \eta \partial(\zeta_t(\mathbf{Y}) + \zeta_{\lambda_t, \mu_t}(\mathbf{Y})) \big|_{\mathbf{Y}=\mathbf{Y}^{t-1}}]_+ \quad (20)$$

where $\partial(\cdot)$ denotes the subgradient operator, and $\eta \geq 0$ is a small constant step-size. A major limitation associated with (20) is that the resulting per-iteration solutions \mathbf{O}^t are generally not sparse. Instead of subgradients, an AM procedure with FISTA updates adopted for \mathbf{O}^t is followed in a manner similar to Algorithms 1 and 2. The main differences stem from eliminating the recursive updates, and adopting constant step sizes to facilitate tracking.

To this end, the following subproblems are solved during interval t ,

$$\mathbf{U}^t = \arg \min_{\mathbf{U} \in \mathbb{R}_+^{N \times C}} \zeta_t(\mathbf{U}, \mathbf{V}^{t-1}, \mathbf{O}^{t-1}, \mathbf{A}^t) + \zeta_{\lambda_t, \mu_t}(\mathbf{U}, \mathbf{V}^{t-1}, \mathbf{O}^{t-1}) \quad (21)$$

$$\mathbf{V}^t = \arg \min_{\mathbf{V} \in \mathbb{R}_+^{N \times C}} \zeta_t(\mathbf{U}^t, \mathbf{V}, \mathbf{O}^{t-1}, \mathbf{A}^t) + \zeta_{\lambda_t, \mu_t}(\mathbf{U}^t, \mathbf{V}, \mathbf{O}^{t-1}) \quad (22)$$

$$\mathbf{O}^t = \arg \min_{\mathbf{O} \in \mathbb{R}_+^{N \times C}} \zeta_t(\mathbf{U}^t, \mathbf{V}^t, \mathbf{O}, \mathbf{A}^t) + \zeta_{\lambda_t, \mu_t}(\mathbf{U}^t, \mathbf{V}^t, \mathbf{O}). \quad (23)$$

In order to operate in real-time, \mathbf{U} and \mathbf{V} can be updated by a single gradient descent step per time slot. Similarly, minimization of (23) across time slots entails a single FISTA update that linearly combines \mathbf{O}^{t-1} and \mathbf{O}^{t-2} . Exact algorithmic details of the SGD-based community tracking algorithm are tabulated in Algorithm 3, with $\Upsilon_t(\mathbf{U}, \mathbf{V}, \mathbf{O}, \mathbf{A}^t) := \zeta_t(\mathbf{U}, \mathbf{V}, \mathbf{O}, \mathbf{A}^t) + \zeta_{\lambda_t, \mu_t}(\mathbf{U}, \mathbf{V}, \mathbf{O})$.

Algorithm 3 SGD tracking algorithm

- 1: **Input:** $\{\mathbf{A}^t\}_{t=1}^T, \beta, C, \alpha_u, \alpha_v$
 - 2: Initialize $\mathbf{U}^0, \mathbf{V}^0, \mathbf{O}^0$
 - 3: Set $\mathbf{W}^0 = \mathbf{O}^0, \theta_0 = 1$
 - 4: **for** $t = 1 \dots T$ **do**
 - 5: $\mathbf{U}^t = [\mathbf{U}^{t-1} - \alpha_u \nabla_{\mathbf{U}} \Upsilon_t(\mathbf{U}, \mathbf{V}^{t-1}, \mathbf{O}^{t-1}, \mathbf{A}^t)]_+$
 - 6: $\mathbf{V}^t = [\mathbf{V}^{t-1} - \alpha_v \nabla_{\mathbf{V}} \Upsilon_t(\mathbf{U}^t, \mathbf{V}, \mathbf{O}^{t-1}, \mathbf{A}^t)]_+$
 - 7: $\mathbf{X}^t = (\mathbf{W}^t - \frac{1}{L_\Phi} \nabla_{\mathbf{O}} \Phi(\mathbf{W}^t, \mathbf{U}^t, \mathbf{V}^t, \mathbf{A}^t, 1))$
 - 8: $\mathbf{O}^t = [\mathcal{S}_{\mu_t/L_\Phi}(\mathbf{X}^t)]_+$
 - 9: $\theta_t = (1 + \sqrt{1 + 4\theta_{t-1}^2})/2$
 - 10: $\mathbf{W}^t = \mathbf{O}^t + ((\theta_{t-1} - 1)/\theta_t)(\mathbf{O}^t - \mathbf{O}^{t-1})$
 - 11: **end for**
-

V. DECENTRALIZED IMPLEMENTATION

The tracking algorithms developed so far have assumed that connectivity data (i.e., $\{\mathbf{A}^t\}$) are acquired and processed in a centralized fashion. This may turn out to be infeasible, since for example, certain applications store large graphs over distributed file storage system hosted across a large network of computers. In fact, graphs capturing the web link structure, and online social networks are typically stored as “chunks” of files that are both distributed across computing nodes, and spatially over several geographical sites. In addition to the inherent computational bottlenecks, soaring data communication costs would render centralized approaches infeasible in such scenarios.

In lieu of these computational constraints, this section puts forth a decentralized algorithm that jointly tracks temporal communities and anomalous nodes. The alternating-direction method of multipliers (ADMM) has recently emerged as powerful tool for decentralized optimization problems [25], and it will be adopted here for the community tracking task. A connected network of computing agents is deployed, with links representing direct communication paths between nodes. The key idea is that each node iteratively solves the problem using only a subset of the input data, while exchanging intermediate solutions with single-hop neighbors until consensus is achieved.

A. Consensus constraints

Consider an undirected graph $\mathcal{G} = (\mathcal{M}, \mathcal{L})$ whose vertices $\mathcal{M} := \{1, \dots, M\}$ are M spatially-distributed computing agents, and whose edges $\mathcal{L} := \{1, \dots, L\}$ are representative of direct communication links between pairs of agents. It is assumed that the processing network abstracted by \mathcal{G} is connected, so that (multi-hop) communication is possible between any pair of agents. Suppose the temporal adjacency matrix is partitioned as follows $\mathbf{A}^t := [(\mathbf{A}_1^t)^\top, \dots, (\mathbf{A}_M^t)^\top]^\top$, and

it is distributed across the processing network. During time interval t , agent m receives the submatrix \mathbf{A}_m^t . To minimize communication costs, each agent is only allowed to send and receive data from its single-hop neighborhood \mathcal{N}_m . Let $\mathbf{U} := [\mathbf{U}_1^\top, \dots, \mathbf{U}_M^\top]^\top$ and $\mathbf{O} := [\mathbf{O}_1^\top, \dots, \mathbf{O}_M^\top]^\top$, where $\mathbf{U}_m \in \mathbb{R}^{N_m \times C}$, $\mathbf{O}_m \in \mathbb{R}^{N_m \times C}$, and $\sum_{m=1}^M N_m = N$. In terms of the per-agent submatrices, (8) can now be written as follows

$$\begin{aligned} & \arg \min_{\substack{\{\mathbf{U}_m, \mathbf{O}_m \in \mathbb{R}_+^{N_m \times C}\}_{m=1}^M \\ \mathbf{V} \in \mathbb{R}_+^{N \times C}}} \sum_{m=1}^M \left[\sum_{\tau=1}^t \beta^{t-\tau} \|\mathbf{A}_m^\tau - (\mathbf{U}_m + \mathbf{O}_m) \right. \\ & \left. \times \mathbf{V}^\top\|_F^2 + \frac{\lambda_t}{2} \|\mathbf{U}_m\|_F^2 + \frac{\lambda_t}{2M} \|\mathbf{V}\|_F^2 + \mu_t \|\mathbf{O}_m\|_1 \right] \quad (24) \end{aligned}$$

for $t = 1, \dots, T$. Clearly \mathbf{U} and \mathbf{O} decouple across computing agents, whereas \mathbf{V} does not. A viable approach entails allowing each agent to solve for its corresponding unknowns \mathbf{U}_m and \mathbf{O}_m in parallel, followed by communication of the estimates to a central processing node that solves for \mathbf{V} . The downside to this approach is that it involves a significant communication and storage overhead as the central node must receive intermediate values of $\{\mathbf{U}_m, \mathbf{O}_m\}_{m=1}^M$, and then broadcast its computed value of \mathbf{V} per iteration. In addition, this introduces the risk of a single point of failure at the central node.

To operate in a truly decentralized manner, each agent will solve for \mathbf{V} independently under *consensus* constraints requiring equality of the solution to those computed by single-hop neighbors [25]. Since \mathcal{G} is connected, it can be readily shown that consensus on the solution for \mathbf{V} will be reached upon convergence of the algorithm [25]. Incorporating consensus constraints, each time interval entails solving the following fully decoupled minimization problem

$$\begin{aligned} & \arg \min_{\{\mathbf{U}_m, \mathbf{O}_m, \mathbf{V}_m\}_{m=1}^M} \sum_{m=1}^M \left[\Phi(\mathbf{U}_m, \mathbf{V}_m, \mathbf{O}_m, \mathbf{S}_m^t, s^t) \right. \\ & \left. + \frac{\lambda_t}{2} \|\mathbf{U}_m\|_F^2 + \frac{\lambda_t}{2M} \|\mathbf{V}_m\|_F^2 + \mu_t \|\mathbf{O}_m\|_1 \right] \\ & \text{s. to } \quad \{\mathbf{U}_m, \mathbf{O}_m\} \in \mathbb{R}_+^{N_m \times C}, \mathbf{V}_m \in \mathbb{R}_+^{N \times C} \\ & \quad \mathbf{V}_m = \mathbf{V}_n, n \in \mathcal{N}_m. \quad (25) \end{aligned}$$

Letting

$$\begin{aligned} \Psi_{\lambda_t}(\mathbf{U}_m, \mathbf{O}_m, \mathbf{V}_m, \mathbf{S}_m^t, s^t) & := \Phi(\mathbf{U}_m, \mathbf{V}_m, \mathbf{O}_m, \mathbf{S}_m^t, s^t) \\ & + \frac{\lambda_t}{2} \|\mathbf{U}_m\|_F^2 + \frac{\lambda_t}{2M} \|\mathbf{V}_m\|_F^2 \quad (26) \end{aligned}$$

and introducing dummy variables $\{\mathbf{P}_m\}_{m=1}^M$, (25) can be written as follows

$$\begin{aligned} & \arg \min_{\{\mathbf{U}_m, \mathbf{O}_m, \mathbf{V}_m\}_{m=1}^M} \sum_{m=1}^M \left[\Psi_{\lambda_t}(\mathbf{U}_m, \mathbf{O}_m, \mathbf{V}_m, \mathbf{S}_m^t, s^t) \right. \\ & \left. + \mu_t \|\mathbf{P}_m\|_1 \right] \\ & \text{s. to } \quad \{\mathbf{U}_m, \mathbf{O}_m\} \in \mathbb{R}_+^{N_m \times C}, \mathbf{V}_m \in \mathbb{R}_+^{N \times C} \\ & \quad \mathbf{O}_m = \mathbf{P}_m, \mathbf{V}_m = \mathbf{V}_n, n \in \mathcal{N}_m. \quad (27) \end{aligned}$$

In order to solve (27), introduce the variables $\{\bar{\mathbf{X}}_{nm}, \tilde{\mathbf{X}}_{nm}\}$, and modify the constraints $\mathbf{V}_m = \mathbf{V}_n, n \in \mathcal{N}_m$ as

$$\mathbf{V}_m = \bar{\mathbf{X}}_{nm}, \mathbf{V}_n = \tilde{\mathbf{X}}_{nm}, \bar{\mathbf{X}}_{nm} = \tilde{\mathbf{X}}_{nm}, n \in \mathcal{N}_m.$$

Introducing the dual variables $\{\Gamma_m\}_{m=1}^M$, and $\{\{\bar{\Pi}_{nm}, \tilde{\Pi}_{nm}\}_{n \in \mathcal{N}_m}\}_{m=1}^M$, and temporarily ignoring non-negativity constraints, the resulting augmented Lagrangian can be written as

$$\begin{aligned} \mathcal{L}_\rho(\mathcal{P}_1, \mathcal{P}_2, \mathcal{P}_3, \mathcal{D}) &= \sum_{m=1}^M \left[\Psi_{\lambda_t}(\mathbf{U}_m, \mathbf{O}_m, \mathbf{V}_m, \mathbf{S}_m^t, s^t) \right. \\ &\quad \left. + \mu_t \|\mathbf{P}_m\|_1 \right] + \sum_{m=1}^M \left[\text{Tr}(\Gamma_m^\top (\mathbf{O}_m - \mathbf{P}_m)) \right. \\ &\quad \left. + \sum_{n \in \mathcal{N}_m} \text{Tr} \left\{ \bar{\Pi}_{nm}^\top (\mathbf{V}_m - \bar{\mathbf{X}}_{nm}) + \tilde{\Pi}_{nm}^\top (\mathbf{V}_n - \tilde{\mathbf{X}}_{nm}) \right\} \right] \\ &\quad + \frac{\rho}{2} \sum_{m=1}^M \left[\|\mathbf{O}_m - \mathbf{P}_m\|_F^2 \right. \\ &\quad \left. + \sum_{n \in \mathcal{N}_m} \left\{ \|\mathbf{V}_m - \bar{\mathbf{X}}_{nm}\|_F^2 + \|\mathbf{V}_n - \tilde{\mathbf{X}}_{nm}\|_F^2 \right\} \right] \quad (28) \end{aligned}$$

where $\rho > 0$, $\mathcal{P}_1 := \{\mathbf{V}_m\}_{m=1}^M$, $\mathcal{P}_2 := \{\mathbf{U}_m, \mathbf{O}_m, \mathbf{P}_m\}_{m=1}^M$, and $\mathcal{P}_3 := \{\{\bar{\mathbf{X}}_{nm}, \tilde{\mathbf{X}}_{nm}\}_{n \in \mathcal{N}_m}\}_{m=1}^M$ denote primal variables, while $\mathcal{D} := \{\Gamma_m, \{\bar{\Pi}_{nm}, \tilde{\Pi}_{nm}\}_{n \in \mathcal{N}_m}\}_{m=1}^M$ denotes the set of dual variables.

Towards applying ADMM to (28), an iterative strategy is pursued, entailing dual variable update as the first step, followed by alternate minimization of $\mathcal{L}_\rho(\mathcal{P}_1, \mathcal{P}_2, \mathcal{P}_3, \mathcal{D})$ over each of the primal variables, while holding the rest fixed to their most recent values. Since $\mathcal{L}_\rho(\mathcal{P}_1, \mathcal{P}_2, \mathcal{P}_3, \mathcal{D})$ is completely decoupled across the M computing agents, the problem can be solved in an entirely decentralized manner. The per-agent updates of the proposed algorithm during iteration k comprise the following steps.

[S1]: Dual variable update.

$$\Gamma_m[k+1] = \Gamma_m[k] + \rho(\mathbf{O}_m[k] - \mathbf{P}_m[k]) \quad (29a)$$

$$\bar{\Pi}_{nm}[k+1] = \bar{\Pi}_{nm}[k] + \rho(\mathbf{V}_m[k] - \bar{\mathbf{X}}_{nm}[k]) \quad (29b)$$

$$\tilde{\Pi}_{nm}[k+1] = \tilde{\Pi}_{nm}[k] + \rho(\mathbf{V}_n[k] - \tilde{\mathbf{X}}_{nm}[k]) \quad (29c)$$

[S2]: Primal variable update.

$$\mathcal{P}_1[k+1] = \arg \min_{\mathcal{P}_1} \mathcal{L}_\rho(\mathcal{P}_1, \mathcal{P}_2[k], \mathcal{P}_3[k], \mathcal{D}[k+1]) \quad (30a)$$

$$\mathcal{P}_2[k+1] = \arg \min_{\mathcal{P}_2} \mathcal{L}_\rho(\mathcal{P}_1[k+1], \mathcal{P}_2, \mathcal{P}_3[k], \mathcal{D}[k+1]) \quad (30b)$$

$$\mathcal{P}_3[k+1] = \arg \min_{\mathcal{P}_3} \mathcal{L}_\rho(\mathcal{P}_1[k+1], \mathcal{P}_2[k+1], \mathcal{P}_3, \mathcal{D}[k+1]) \quad (30c)$$

It can be shown that the splitting variables in \mathcal{P}_3 turn out to be redundant in the final algorithm. Letting $\bar{\Pi}_m[k] := \sum_{n \in \mathcal{N}_m} \bar{\Pi}_{nm}[k]$, it turns out that

$$\bar{\Pi}_m[k+1] = \bar{\Pi}_m[k] + (\rho/2) \left(|\mathcal{N}_m| \mathbf{V}_m[k] - \sum_{n \in \mathcal{N}_m} \mathbf{V}_n[k] \right) \quad (31)$$

and the dual variables $\tilde{\Pi}_{nm}$ can be discarded. In addition, the per-iteration primal variable updates per agent simplify to (see Appendix A for derivations):

$$\begin{aligned} \mathbf{V}_m[k+1] &= \arg \min_{\mathbf{V}_m \in \mathbb{R}_+^{N \times C}} \Psi_{\lambda_t}(\mathbf{U}_m[k], \mathbf{O}_m[k], \mathbf{V}_m, \mathbf{S}_m^t, s^t) \\ &\quad + \text{Tr}[(\rho/2)|\mathcal{N}_m| \mathbf{V}_m^\top \mathbf{V}_m + \mathbf{V}_m^\top (\bar{\Pi}_m[k+1] \\ &\quad - (\rho/2)\{|\mathcal{N}_m| \mathbf{V}_m[k] + \sum_{n \in \mathcal{N}_m} \mathbf{V}_n[k]\})] \quad (32) \end{aligned}$$

$$\begin{aligned} \mathbf{U}_m[k+1] &= \arg \min_{\mathbf{U}_m \in \mathbb{R}_+^{N_m \times C}} \Psi_{\lambda_t}(\mathbf{U}_m, \mathbf{O}_m[k], \mathbf{V}_m[k+1], \mathbf{S}_m^t, s^t) \quad (33) \end{aligned}$$

$$\begin{aligned} \mathbf{O}_m[k+1] &= \arg \min_{\mathbf{O}_m \in \mathbb{R}_+^{N_m \times C}} \Psi_{\lambda_t}(\mathbf{U}_m[k+1], \mathbf{O}_m, \mathbf{V}_m[k+1], \mathbf{S}_m^t, s^t) \\ &\quad + \text{Tr}(\Gamma_m^\top[k+1] \mathbf{O}_m) + (\rho/2) \|\mathbf{O}_m - \mathbf{P}_m[k]\|_F^2 \quad (34) \end{aligned}$$

$$\begin{aligned} \mathbf{P}_m[k+1] &= \arg \min_{\mathbf{P}_m \in \mathbb{R}_+^{N_m \times C}} (\rho/2) \|\mathbf{O}_m[k+1] - \mathbf{P}_m\|_F^2 \\ &\quad - \text{Tr}(\Gamma_m^\top[k+1] \mathbf{P}_m) + \mu_t \|\mathbf{P}_m\|_1. \quad (35) \end{aligned}$$

Algorithm 4 summarizes the steps involved in the per-agent decentralized ADMM algorithm.

Algorithm 4 Decentralized tracking algorithm per agent m

- 1: **Input:** $\{\mathbf{A}_m^t\}_{t=1}^T, \beta, C, \rho$
- 2: $\mathbf{U}_m^0, \mathbf{V}_m^0, \mathbf{O}_m^0 = \mathbf{P}_m^0 = \mathbf{0}$
- 3: $\bar{\Pi}_m^0[0] = \mathbf{0}, \Gamma_m^0[0] = \mathbf{0}$
- 4: **for** $t = 1 \dots T$ **do**
- 5: Set $s^t = (1 - \beta^t)/(1 - \beta)$
- 6: Update $\mathbf{S}_m^t = \mathbf{A}_m^t + \beta \mathbf{S}_m^{t-1}$
- 7: Update μ_t and λ_t
- 8: $\mathbf{V}_m[0] = \mathbf{V}_m^{t-1}, \mathbf{U}_m[0] = \mathbf{U}_m^{t-1}$
- 9: $\mathbf{O}_m[0] = \mathbf{P}_m[0] = \mathbf{O}_m^{t-1}, k = 0$
- 10: **repeat**
- 11: Receive $\{\mathbf{V}_n[k]\}_{n \in \mathcal{N}_m}$ from neighbors of m
- 12: $\Gamma_m[k+1] = \Gamma_m[k] + \rho(\mathbf{O}_m[k] - \mathbf{P}_m[k])$
- 13: Compute $\bar{\Pi}_m[k+1]$ according to (31)
- 14: Update $\mathbf{V}_m[k+1]$ via (32)
- 15: Update $\mathbf{U}_m[k+1]$ via (33)
- 16: Update $\mathbf{O}_m[k+1]$ via (34)
- 17: Update $\mathbf{P}_m[k+1]$ via (35)
- 18: Broadcast $\mathbf{V}_m[k+1]$ to single-hop neighbors
- 19: $k = k + 1$
- 20: **until** $\mathbf{U}_m[k], \mathbf{V}_m[k], \mathbf{O}_m[k]$ converge
- 21: $\mathbf{U}_m^t = \mathbf{U}_m[k], \mathbf{V}_m^t = \mathbf{V}_m[k], \mathbf{O}_m^t = \mathbf{O}_m[k]$
- 22: **end for**

VI. SIMULATIONS

A. Synthetic Data

Data generation. An initial synthetic network with $N = 100$, and $C = 5$ communities was generated using the stochastic

blockmodel (SBM) [15]. The SBM parameters were set to: $\delta_{ii} = 0.8, i = 1, \dots, 5$, and $\delta_{ij} \in \{0, 0.1\}, i \neq j$, selected so that the SBM matrix is stochastic (see Figure 2(a)). The initial SBM network was captured through an adjacency matrix $\mathbf{A}^{\text{init}} \in \{0, 1\}^{N \times N}$. Matrix \mathbf{A}^{init} was then decomposed into non-negative factors \mathbf{U}^0 and \mathbf{V}^0 , that is, $\mathbf{A}^{\text{init}} = \mathbf{U}^0(\mathbf{V}^0)^\top$, using standard off-the-shelf NMF tools. Anomalies were artificially induced by reconstructing a modified adjacency matrix $\mathbf{A}^0 = (\mathbf{U}^0 + \mathbf{O}^0)(\mathbf{V}^0)^\top$, where the only non-zero rows of \mathbf{O}^0 are indexed by $\{0, 25, 30, 80\}$. Figure 2 depicts a heatmap of \mathbf{A}^0 , clearly showing anomalous nodes as unusually highly connected.

In order to generate slowly evolving networks, four piecewise constant edge-variation functions were adopted: i) $f_1(t) = H(t)$; ii) $f_2(t) = H(t-50)$; iii) $f_3(t) = 1 - H(t-50)$; and iv) $f_4(t) = H(t) - H(t-25) + H(t-50) - H(t-75)$, where $H(t)$ denotes the unit step function, and $t = 1, \dots, 100$. The time-series $\{\mathbf{A}^t\}_{t=1}^{100}$ was generated by setting the edge indicators to $a_{ij}^t = a_{ij}^0 f_\kappa(t)$, with κ uniformly selected at random from $\{1, 2, 3, 4\}$.

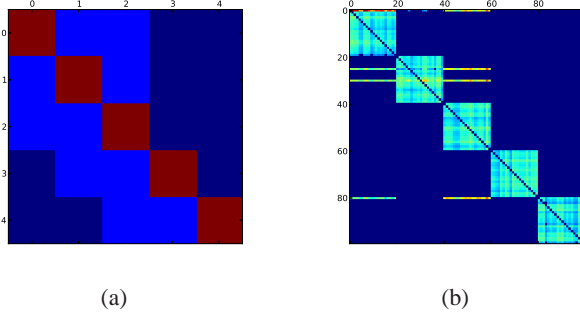


Fig. 2: a) SBM matrix for community generation with parameters $\delta_{ij} \in \{0, 0.1, 0.8\}$, decreasing away from the diagonal; b) Heatmap of the initial network with anomalous nodes at rows $\{0, 25, 30, 80\}$.

Numerical results. Algorithm 1 was initialized by setting \mathbf{O} to an all-zero matrix, while \mathbf{U} and \mathbf{V} were initialized to NMF factors of \mathbf{A}^0 computed in batch. With $K = 5$ and $\beta = 0.97$, Algorithm 1 was run to track the constituent communities and anomalies. Selection of λ_t and μ_t is admittedly challenging under dynamic settings where data are sequentially acquired. Nevertheless, heuristics such as increasing μ_t over time work reasonably well when the unknowns vary slowly. It turns out that setting $\lambda_t = 0.05$, and $\mu_t = 0.1\sqrt{t}$ yielded remarkably good community tracking. Generally, 8 – 10 inner iterations sufficed for convergence per time step. Figure 3 depicts stacked plots of community affiliation strengths against node indices, over a selected sample of intervals. Despite the community overlaps unveiled by the algorithm, it is clear that all nodes generally exhibit strong affiliation with one of the five communities.

Hard community assignment was done by associating node i with community m , where $m = \arg \max_k \hat{u}_{ik}$. Figure 5 depicts visualizations of the network at $t = 10, 40$, and 70 , with node colors reflecting identified community membership per time interval. Nodes flagged off as anomalies are shown

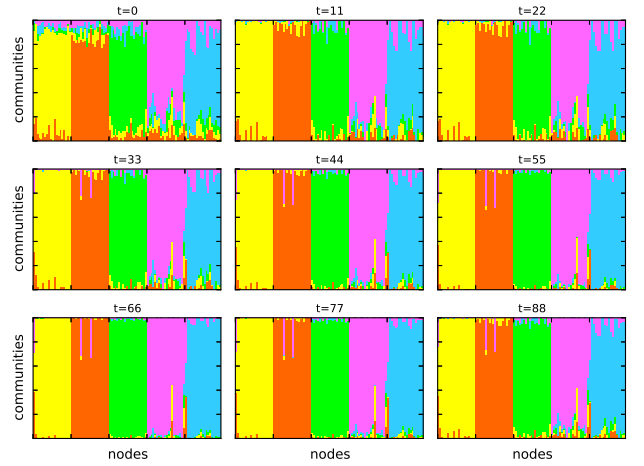


Fig. 3: Stacked plots depicting overlapping communities detected over a selected sample of time intervals. Horizontal axes are indexed by nodes, while vertical axes depict community affiliation strengths that are proportional to the relative dominance of each color per node. As expected, most nodes exhibit a strong affiliation with one of the five communities.

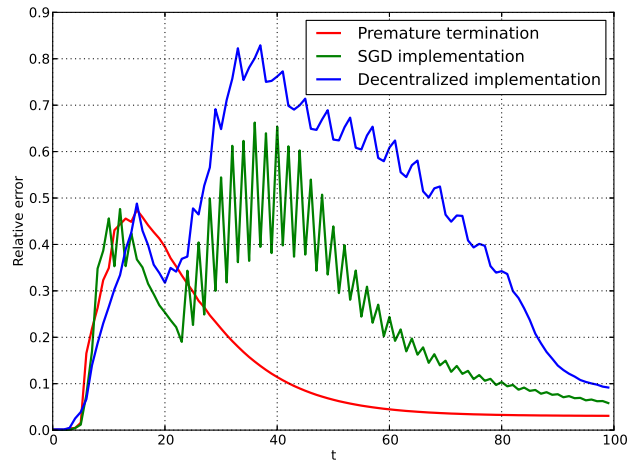


Fig. 4: Comparison of the relative error performance of developed algorithms with parameters set to $\lambda_0 = 0.05, \mu_0 = 0.1, \beta = 0.97$.

with larger node sizes and explicit labels. Initially the set of detected anomalies includes a number of false alarms. With acquisition of more sequential data, the algorithm is able to iteratively prune the set, until the ground-truth anomalies are identified (Figure 5 (c)).

Further tests were conducted with Algorithms 2, 3, and 4. For the decentralized implementation, a simple connected network of 10 computing agents was adopted, as shown in Figure 8. Figure 4 plots the relative error with respect to batch solutions, resulting from running the algorithms using the synthetic network time-series. The relative error during interval t is computed as

$$\frac{\|\hat{\mathbf{U}}^t - \hat{\mathbf{U}}_{\text{batch}}^t\|_F + \|\hat{\mathbf{V}}^t - \hat{\mathbf{V}}_{\text{batch}}^t\|_F + \|\hat{\mathbf{O}}^t - \hat{\mathbf{O}}_{\text{batch}}^t\|_F}{\|\hat{\mathbf{U}}_{\text{batch}}^t\|_F + \|\hat{\mathbf{V}}_{\text{batch}}^t\|_F + \|\hat{\mathbf{O}}_{\text{batch}}^t\|_F}$$

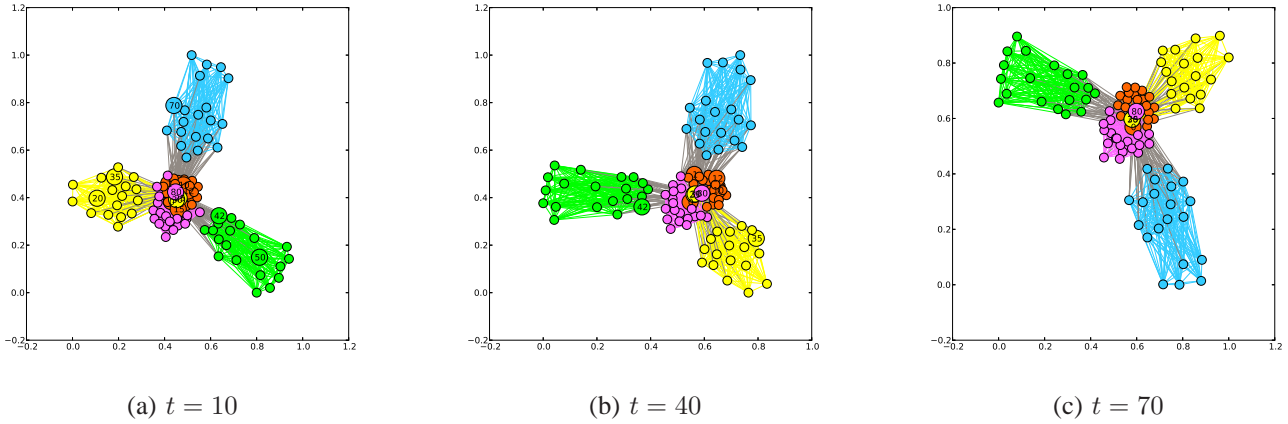


Fig. 5: Visualization of the largest connected components with artificially-induced anomalies at $t = 10, 40, 70$. Node colors indicate detected communities, and anomalous members are depicted by larger node sizes with labels. Although no anomalies were initially detected, further data acquisition facilitated convergence to the correct set of anomalies, i.e., $\{0, 25, 30, 80\}$.

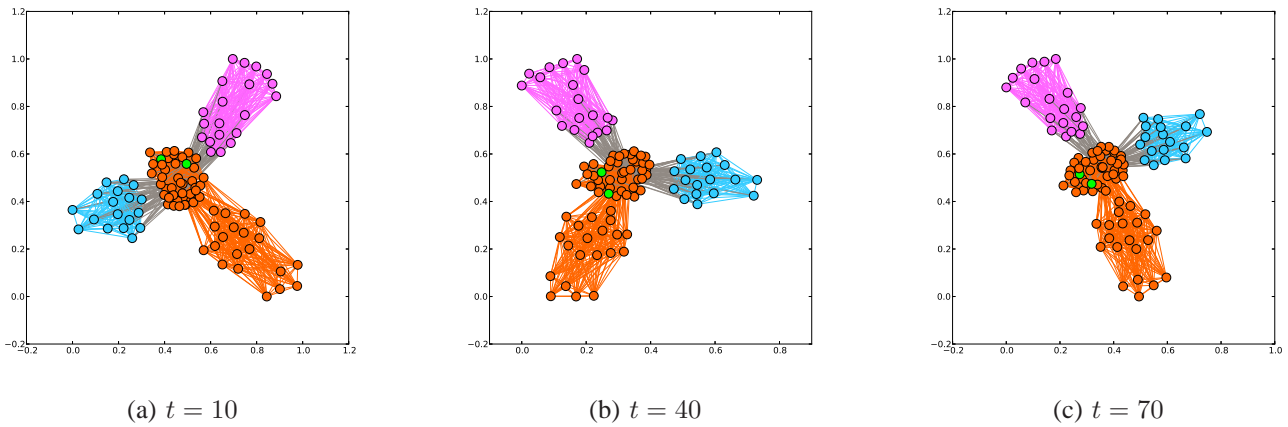


Fig. 6: Demonstration of the distortive effect of anomalies with respect to community structure. Plots (a)-(c) demonstrate the results of running a standard outlier-agnostic algorithm, with the inaccurate conclusion that the time-series is dominated by three communities.

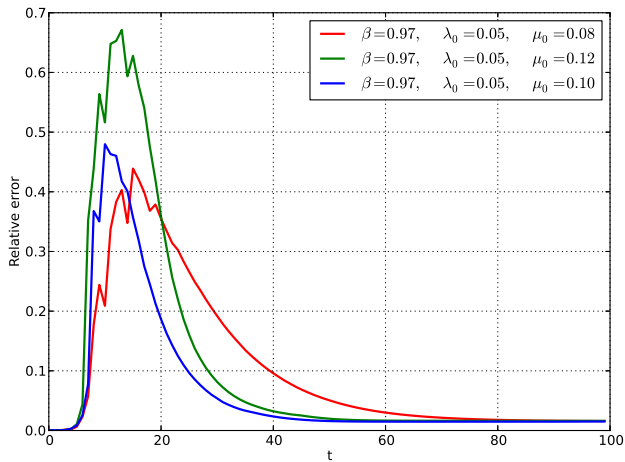


Fig. 7: Comparison of relative error plots resulting from running Algorithm 1 and varying μ_0 .

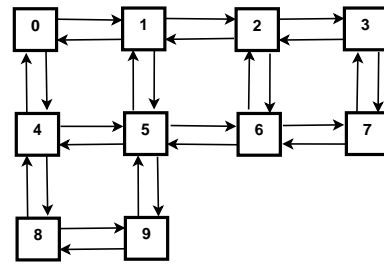


Fig. 8: A simple connected network of 10 computing agents used for the decentralized community tracking task.

where \hat{U}_{batch}^t is the batch solution per interval t . With initial batch solutions, relative errors are initially small, followed by dramatic increases upon acquisition of sequential data. As more data are acquired, tracking with premature termination leads to faster error decay than the SGD alternative, presumably because it directly incorporates all past data by recursive aggregation. Decentralized iterations yield the slowest decay, because in addition to seeking convergence to the batch solu-

	Country	Years as anomaly
1	German Federal Republic	1954, 1955, 1956, 1966
2	Russia	1953, 1954, 1955, 1956
3	Austria	1955, 1957, 1960
4	Pakistan	1955, 1956, 1957
5	Japan	1954, 1955, 1965, 1967
6	South Korea	1955, 1965
7	Yugoslavia	1954, 1956
8	Iraq	1967
9	Yemen Arab Republic	1964, 1965
10	Kenya	1966, 1968

TABLE I: Anomalous countries in the global trade dataset.

tion, consensus per agent must be attained per time-interval.

Selection of μ_t is critical for joint identification of anomalies, as it controls the sparsity level inherent to \mathbf{O}^t . Although this is very challenging in time-varying settings, empirical investigation was used to guide selection of the “best” initial parameter μ_0 . Figure 7 plots the relative error (with respect to batch solutions) resulting from running Algorithm 1 for several values of μ_0 , with $\beta = 0.97$, and $\lambda_t = \lambda_0 = 0.05$ for all t . As seen from the plots, setting $\mu_0 = 0.10$ led to the fastest convergence to the batch solutions.

B. Real Data

Dataset description. The developed algorithms were tested on a time-series of real-world networks extracted from global trade flow statistics. Extracted under the *Correlates of War* project [3], the dataset captures information on annual bilateral trade flows (imports and exports) among countries between 1870 and 2009. The network time-series were indexed by trade years, and each node was representative of a country, while directed and weighted edges were indicative of the volume and direction (export/import) of trade between countries measured in present-day U.S. dollars.

Since trade volumes between countries can vary by orders of magnitude, edge weights were set to logarithms of the recorded trade flows. It is also important to note that some countries did not exist until 50 or fewer years ago. As a result, network dynamics in the dataset were due to arrival and obsolescence of some nodes, in addition to annual changes in edges and their weights. Since this paper assumes that a fixed set of nodes is available, the tracking algorithm was run for data ranging from 1949 to 2009 (i.e., $T = 60$), with $N = 170$ countries.

The objective of this experiment was to track the evolution of communities within the global trade network, and to identify any anomalies. Note that communities in the world trade network may be interpreted as regional trading consortia. Algorithm 3 was run with $C = 7$ communities, $\beta = 0.97$, $\alpha_u = \alpha_v = 0.002$, $\lambda_t = 0.5$, and $\mu_t = 1.0$, for all $t = 1, \dots, T$. Initial values \mathbf{U}^0 and \mathbf{V}^0 were obtained by traditional NMF on \mathbf{A}^0 , and \mathbf{O}^0 was set to an all-zero $N \times C$ matrix.

Numerical results. Running Algorithm 3 on this dataset revealed interesting insights about the evolution of global trade within the last sixty years. Figure 9 depicts stacked plots of countries and the communities they belonged to over a subset of years within the observation period. The horizontal axes are

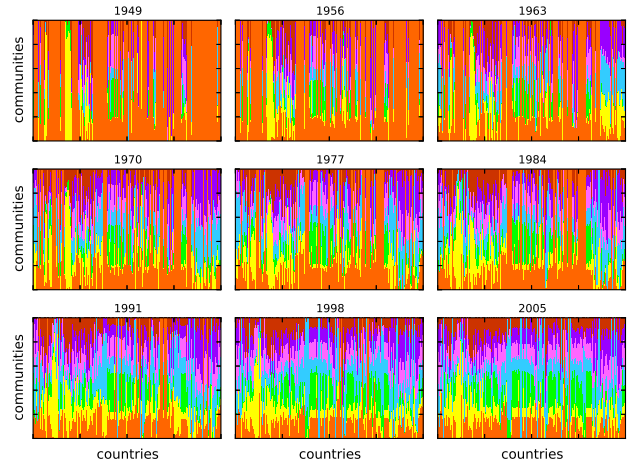


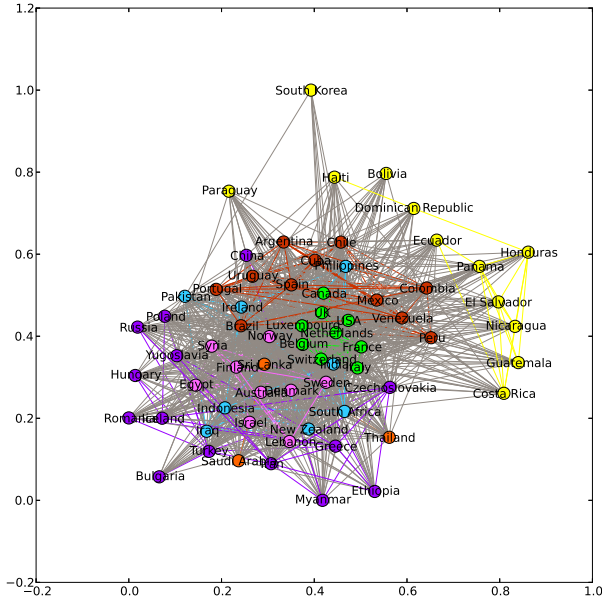
Fig. 9: Overlapping communities in world trade flows dataset. The bottom row of plots suggests a growing trend of globalization, with most countries participating in several trade communities.

indexed by countries, and each community is depicted by a specific color. It is clear that over the years, more countries cultivated stronger affiliations within different communities. This observation suggests an increasing trend of globalization, with more countries actively engaging in significant trade relationships within different trade communities. Between 1949 and 1963, global trade was dominated by one major community, while the other communities played a less significant role. Based on historical accounts, it is likely that such trade dynamics were related to ongoing global recovery in the years following the second world war.

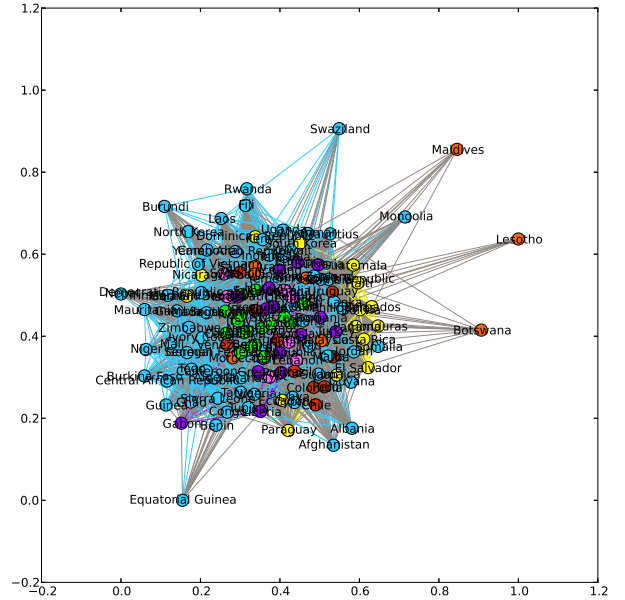
Figure 10 depicts visualizations of the global trade network for the years 1959 and 1990, with countries color-coded according to the community with which they are most strongly affiliated. A core community of economic powerhouses (in green) comprises global leaders such as the United States, United Kingdom, Canada, France etc., as seen from the 1959 visualization. Interestingly, this core group of countries remains intact as a community in 1990. It turns out that geographical proximity and language play an important role in trade relationships. This is evident from two communities (colored maroon and yellow) which are dominated by South and Central American nations, with Spain and Portugal as exceptions that have strong cultural and language influences on these regions.

Another interesting observation from the 1990 visualization is the large community of developing nations (in blue). Most of these nations only existed as colonies in 1959, and are not depicted in the first drawing. However, 1990 lies within their post-colonial period, during which they presumably started establishing strong trading ties with one another.

Finally, Table I lists countries that were flagged off by Algorithm 3 as anomalies. The table shows each of these countries, along with a list of years during which they were identified as anomalies. In the context of global trade, anomalies are expected to indicate abnormal or irregular trading patterns. Interestingly, the German Federal Republic, Russia, and Japan were some of the most adversely affected countries by the



(a) 1959



(b) 1990

Fig. 10: Communities identified in the global trade network for the years 1959 and 1990.

second world war, and their trade patterns during a period of rapid economic revival may corroborate identification as anomalies. It is also possible that South Korea was flagged off in 1955 and 1965 because of its miraculous economic growth that started in the 1950s.

VII. CONCLUSION

This paper put forth a novel approach for jointly tracking communities in time-varying network settings, and identifying anomalous members. Leveraging advances in overlapping community discovery, a temporal outlier-aware edge generation model was proposed. It was assumed that the anomaly matrix is sparse, the outlier-free, noiseless factor model is low rank, and the network evolves slowly. Based on these assumptions, a sparsity-promoting, rank-regularized EWLSE was advocated to jointly track communities and identify anomalous nodes. A first-order sequential tracking algorithm was developed, based on alternating minimization and recent advances in accelerated proximal-splitting optimization.

Motivated by contemporary needs for processing big data, often in streaming and distributed settings, a number of algorithmic improvements were put forth. Real-time operation was attained by developing a fast online tracking algorithm, based on stochastic gradient iterations. For settings involving distributed acquisition and storage of network data, a decentralized tracking algorithm that capitalizes on the separability inherent to ADMM iterations was developed.

Simulations on synthetic SBM networks successfully unveiled the underlying communities, and flagged off artificially-induced anomalies. Experiments conducted on a sequence of networks extracted from historical global trade flows between

nations revealed interesting results concerning globalization of trade, and unusual trading behavior exhibited by certain countries during the early post-world war era.

APPENDIX A

DERIVATION OF DECENTRALIZED UPDATES

Recalling the constraint $\bar{\mathbf{X}}_{nm} = \tilde{\mathbf{X}}_{nm}$, the per-iteration update in (30c) becomes

$$\begin{aligned} \bar{\mathbf{X}}_{nm}[k+1] = \arg \min_{\bar{\mathbf{X}}_{nm}} & \frac{\rho}{2} \left\{ \|\mathbf{V}_m[k+1] - \bar{\mathbf{X}}_{nm}\|_F^2 \right. \\ & \left. + \|\mathbf{V}_n[k+1] - \bar{\mathbf{X}}_{nm}\|_F^2 \right\} \\ & - \text{Tr} \left\{ \left(\bar{\mathbf{\Pi}}_{nm}[k+1] + \tilde{\mathbf{\Pi}}_{nm}[k+1] \right)^\top \bar{\mathbf{X}}_{nm} \right\} \end{aligned} \quad (36)$$

whose solution turns out to be

$$\begin{aligned} \bar{\mathbf{X}}_{nm}[k+1] = \frac{1}{2\rho} & \left(\bar{\mathbf{\Pi}}_{nm}[k+1] + \tilde{\mathbf{\Pi}}_{nm}[k+1] \right) \\ & + \frac{1}{2} \left(\mathbf{V}_m[k+1] + \mathbf{V}_n[k+1] \right). \end{aligned} \quad (37)$$

Assuming that $\bar{\mathbf{\Pi}}_{nm}[0] = -\tilde{\mathbf{\Pi}}_{nm}[0]$, then it can be shown by a simple inductive argument that $\bar{\mathbf{\Pi}}_{nm}[k] = -\tilde{\mathbf{\Pi}}_{nm}[k], n \in \mathcal{N}_m$ [21]. Consequently,

$$\bar{\mathbf{X}}_{nm}[k] = \frac{1}{2} \left(\mathbf{V}_m[k] + \mathbf{V}_n[k] \right) \quad (38)$$

and

$$\bar{\mathbf{\Pi}}_{nm}[k+1] = \bar{\mathbf{\Pi}}_{nm}[k] + \frac{\rho}{2} \left(\mathbf{V}_m[k] - \mathbf{V}_n[k] \right). \quad (39)$$

Due to (38), note that $\bar{\mathbf{X}}_{nm}[k] = \bar{\mathbf{X}}_{mn}[k], n \in \mathcal{N}_m$, and that if $\bar{\mathbf{\Pi}}_{nm}[0] = -\bar{\mathbf{\Pi}}_{mn}[0]$, then $\bar{\mathbf{\Pi}}_{nm}[k] = -\bar{\mathbf{\Pi}}_{mn}[k], n \in \mathcal{N}_m$.

Focusing on the update for \mathbf{V}_m in (30a), and dropping the irrelevant terms yields

$$\begin{aligned} \arg \min_{\mathbf{V}_m} \Psi_{\lambda_t}(\mathbf{U}_m[k], \mathbf{O}_m[k], \mathbf{V}_m, \mathbf{S}_m^t, s^t) \\ + \text{Tr} \left\{ \sum_{n \in \mathcal{N}_m} (\bar{\mathbf{\Pi}}_{nm}^\top[k+1](\mathbf{V}_m - \bar{\mathbf{X}}_{nm}[k])) \right\} \\ + \frac{\rho}{2} \sum_{n \in \mathcal{N}_m} \|\mathbf{V}_m - \bar{\mathbf{X}}_{nm}[k]\|_F^2. \end{aligned} \quad (40)$$

Eliminating constants in the second term, one obtains

$$\text{Tr} \left\{ \sum_{n \in \mathcal{N}_m} \bar{\mathbf{\Pi}}_{nm}^\top[k+1] \mathbf{V}_m \right\} = \text{Tr} \left\{ \mathbf{V}_m^\top \bar{\mathbf{\Pi}}_m[k+1] \right\} \quad (41)$$

where $\bar{\mathbf{\Pi}}_m[k+1] := \sum_{n \in \mathcal{N}_m} \bar{\mathbf{\Pi}}_{nm}[k+1]$. Using (39),

$$\begin{aligned} \sum_{n \in \mathcal{N}_m} \bar{\mathbf{\Pi}}_{nm}[k+1] &= \sum_{n \in \mathcal{N}_m} \bar{\mathbf{\Pi}}_{nm}[k] \\ &+ \frac{\rho}{2} \left(|\mathcal{N}_m| - \sum_{n \in \mathcal{N}_m} \mathbf{V}_n[k] \right) \end{aligned} \quad (42)$$

leading to the dual variable update

$$\bar{\mathbf{\Pi}}_m[k+1] = \bar{\mathbf{\Pi}}_m[k] + \frac{\rho}{2} \left(|\mathcal{N}_m| - \sum_{n \in \mathcal{N}_m} \mathbf{V}_n[k] \right). \quad (43)$$

Expansion of the third term in (40) leads to

$$\begin{aligned} \frac{\rho}{2} \sum_{n \in \mathcal{N}_m} \|\mathbf{V}_m - \bar{\mathbf{X}}_{nm}[k]\|_F^2 = \\ \frac{\rho}{2} \text{Tr} \left\{ |\mathcal{N}_m| \mathbf{V}_m^\top \mathbf{V}_m - 2 \mathbf{V}_m^\top \sum_{n \in \mathcal{N}_m} \bar{\mathbf{X}}_{nm} \right\} \end{aligned} \quad (44)$$

and (38) can be used to further expand $\sum_{n \in \mathcal{N}_m} \bar{\mathbf{X}}_{nm}$ as follows

$$\sum_{n \in \mathcal{N}_m} \bar{\mathbf{X}}_{nm} = \frac{|\mathcal{N}_m|}{2} \mathbf{V}_m[k] + \frac{1}{2} \sum_{n \in \mathcal{N}_m} \mathbf{V}_n[k]. \quad (45)$$

Upon substituting (45) into (44), it turns out that

$$\begin{aligned} \frac{\rho}{2} \sum_{n \in \mathcal{N}_m} \|\mathbf{V}_m - \bar{\mathbf{X}}_{nm}[k]\|_F^2 = \frac{\rho}{2} \text{Tr} \left\{ |\mathcal{N}_m| \mathbf{V}_m^\top \mathbf{V}_m \right. \\ \left. - 2 \mathbf{V}_m^\top \left(|\mathcal{N}_m| \mathbf{V}_m[k] + \sum_{n \in \mathcal{N}_m} \mathbf{V}_n[k] \right) \right\} \end{aligned} \quad (46)$$

and $\mathbf{V}_m[k+1]$ can be obtained by solving

$$\begin{aligned} \mathbf{V}_m[k+1] = \arg \min_{\mathbf{V}_m \in \mathbb{R}_+^{N \times C}} \Psi_{\lambda_t}(\mathbf{U}_m[k], \mathbf{O}_m[k], \mathbf{V}_m, \mathbf{S}_m^t, s^t) \\ + \text{Tr} \left[(\rho/2) |\mathcal{N}_m| \mathbf{V}_m^\top \mathbf{V}_m + \mathbf{V}_m^\top (\bar{\mathbf{\Pi}}_m[k+1] \right. \\ \left. - (\rho/2) \{ |\mathcal{N}_m| \mathbf{V}_m[k] + \sum_{n \in \mathcal{N}_m} \mathbf{V}_n[k] \} \right] \end{aligned} \quad (47)$$

whose closed-form solution is readily available. The remaining updates for $\mathbf{U}_m[k+1]$, $\mathbf{O}_m[k+1]$, and $\mathbf{P}_m[k+1]$ follow

in a straightforward manner from the ADMM primal variable updates, and they are all available in closed form. Note that solving for $\mathbf{P}_m[k+1]$ entails completion of squares, resulting in a standard Lasso problem whose per-entry solutions are available in closed form using the *soft thresholding* operator.

REFERENCES

- [1] S. Asur, S. Parthasarathy, and D. Ucar, "An event-based framework for characterizing the evolutionary behavior of interaction graphs," *ACM Trans. on Knowledge Discovery from Data*, vol. 3, no. 4, pp. 1–36, Nov. 2009.
- [2] L. Backstrom, D. Huttenlocher, J. Kleinberg, and X. Lan, "Group formation in large social networks: Membership, growth, and evolution," in *Proc. of the 12th ACM SIGKDD Intl. Conf. on Knowledge Discovery and Data Mining*, Philadelphia, PA, Aug. 2006.
- [3] K. Barbieri, O. M. G. Keshk, and B. Pollins, "Trading data: Evaluating our assumptions and coding rules," *Conflict Management and Peace Science*, vol. 26, no. 5, pp. 471–491, Nov. 2009.
- [4] A. Beck and M. Teboulle, "A fast iterative shrinkage-thresholding algorithm for linear inverse problems," *SIAM J. Imag. Sci.*, vol. 2, pp. 183–202, Jan. 2009.
- [5] D. P. Bertsekas, *Nonlinear Programming*. Belmont, MA: Athena Scientific, 1999.
- [6] Y. Chen, Y. Gu, and A. O. Hero III, "Sparse LMS for system identification," in *Proc. of Intern. Conf. on Acoustics, Speech and Signal Processing*, Taipei, Taiwan, Apr. 2009.
- [7] D. M. Dunlavy, T. G. Kolda, and E. Acar, "Temporal link prediction using matrix and tensor factorizations," *ACM Transactions on Knowledge Discovery from Data*, vol. 5, no. 2, pp. 1–10, Feb. 2011.
- [8] D. Easley and J. Kleinberg, *Networks, Crowds, and Markets: Reasoning About a Highly Connected World*. New York, NY: Cambridge University Press, 2010.
- [9] S. Fortunato, "Community detection in graphs," *Physics Reports*, vol. 486, no. 3, pp. 75–174, Feb. 2010.
- [10] W. Fu, L. Song, and E. P. Xing, "Dynamic mixed membership block-model for evolving networks," in *Proc. of the 26th Annual International Conference on Machine Learning*, Montreal, Canada, Jun. 2009.
- [11] G. B. Giannakis, G. Mateos, S. Farahmand, and H. Zhu, "USPACOR: Universal sparsity-controlling outlier rejection," in *Proc. of Intl. Conf. on Acoustics, Speech and Signal Processing*, Prague, Czech Republic, May 2011.
- [12] M. Girvan and M. E. J. Newman, "Community structure in social and biological networks," *Proceedings of the National Academy of Sciences*, vol. 99, pp. 7821–7826, Jun. 2002.
- [13] D. Greene, D. Doyle, and P. Cunningham, "Tracking the evolution of communities in dynamic social networks," in *Proc. of Intl. Conf. on Advances in Social Networks Analysis and Mining*, Odense, Denmark, Aug. 2010.
- [14] T. Hastie, R. Tibshirani, and J. Friedman, *The Elements of Statistical Learning*, 2nd ed. New York, NY: Springer, 2009.
- [15] P. W. Holland, K. B. Laskey, and S. Leinhardt, "Stochastic blockmodels: First steps," *Social Networks*, vol. 5, no. 2, pp. 109–137, 1983.
- [16] S. C. Johnson, "Hierarchical clustering schemes," *Psychometrika*, vol. 32, no. 3, pp. 241–254, 1967.
- [17] E. D. Kolaczyk, *Statistical Analysis of Network Data: Methods and Models*. New York, NY: Springer, 2009.
- [18] Y. R. Lin, Y. Chi, S. Zhu, H. Sundaram, and B. L. Tseng, "Analyzing communities and their evolutions in dynamic social networks," *ACM Trans. on Knowledge Discovery from Data*, vol. 3, no. 2, pp. 1–31, Apr. 2009.
- [19] U. V. Luxburg, "A tutorial on spectral clustering," *Statistics and Computing*, vol. 17, no. 4, pp. 395–416, Dec. 2007.
- [20] S. Mankad and G. Michailidis, "Structural and functional discovery in dynamic networks with non-negative matrix factorization," *Physical Review E*, vol. 88, no. 4, p. 042812, Oct. 2013.
- [21] M. Mardani, G. Mateos, and G. B. Giannakis, "Decentralized sparsity-regularized rank minimization: Algorithms and applications," *IEEE Transactions on Signal Processing*, vol. 61, pp. 5374–5388, Nov. 2013.
- [22] M. E. J. Newman, "Modularity and community structure in networks," *Proc. of the Natl. Academy of Sciences*, vol. 103, no. 23, pp. 8577–8582, Jun. 2006.
- [23] S. Papadimitriou, J. Sun, and C. Faloutsos, "Streaming pattern discovery in multiple time-series," in *Proc. of the 31st Intl. Conf. on Very Large Data Bases*, Trento, Italy, Oct. 2005.

- [24] R. A. Rossi, B. Gallagher, J. Neville, and K. Henderson, "Modeling dynamic behavior in large evolving graphs," in *Proc. of 6th ACM Intl. Conf. on Web Search and Data Mining*, Rome, Italy, Feb. 2013.
- [25] I. D. Schizas, A. Ribeiro, and G. B. Giannakis, "Consensus in ad hoc WSNs with noisy links - Part I: Distributed estimation of deterministic signals," *IEEE Transactions on Signal Processing*, vol. 56, pp. 350–364, Jan. 2008.
- [26] V. Solo and X. Kong, *Adaptive Signal Processing Algorithms: Stability and Performance*. Prentice Hall, 1995.
- [27] J. Sun, C. Faloutsos, S. Papadimitriou, and P. S. Yu, "Graphscope: Parameter-free mining of large time-evolving graphs," in *Proc. of the 13th ACM SIGKDD Intl. Conf. on Knowledge Discovery and Data Mining*, San Jose, CA, Aug. 2007.
- [28] L. Tang, H. Liu, J. Zhang, and Z. Nazeri, "Community evolution in dynamic multi-mode networks," in *Proc. of the 14th ACM SIGKDD Intl. Conf. on Knowledge Discovery and Data Mining*, Las Vegas, NV, Aug. 2008.
- [29] K. S. Xu and A. O. Hero, "Dynamic stochastic blockmodels for time-evolving social networks," *IEEE Journal on Selected Topics in Signal Processing*, vol. 8, no. 4, pp. 552–562, Aug. 2014.
- [30] J. Yang and J. Leskovec, "Overlapping community detection at scale: A nonnegative matrix factorization approach," in *Proc. of 6th ACM Intl. Conf. on Web Search and Data Mining*, Rome, Italy, Feb. 2013.